Black Carbon and Ozone Variability at the Kathmandu Valley and at the Southern Himalayas: A Comparison between a "Hot Spot" and a Downwind High-Altitude Site

Davide Putero[1*], Angela Marinoni[1], Paolo Bonasoni[1], Francescopiero Calzolari[1], Maheswar Rupakheti[2], Paolo Cristofanelli[1]

[1] *National Research Council of Italy – Institute of Atmospheric Sciences and Climate, CNR–ISAC, 40129 Bologna, Italy*
[2] *Institute for Advanced Sustainability Studies, IASS, 14467 Potsdam, Germany*

ABSTRACT

Several studies have reported the transport of short-lived climate forcers/pollutants (SLCF/P) from the highly polluted areas in southern Asia (e.g., the Indo-Gangetic Plain and the Himalayan foothills) to the Himalayas, with significant implications for the global and regional climate, crop yields, and human health. In this work, we perform a comparison of nearly three years (February 2013–October 2015) of simultaneous black carbon (BC) and surface ozone (O_3) measurements at two sites in Nepal, viz., Paknajol (1380 m a.s.l.), in the Kathmandu Valley, and the WMO/GAW global station Nepal Climate Observatory-Pyramid (NCO-P, 5079 m a.s.l.), near the base camp of Mt. Everest. The two sites are only 150 km apart and are characterized by different situations: While the Kathmandu Valley is one of the regional urban "hot spots" for concerns related to air pollution, NCO-P is representative of the background conditions of the high Himalayas and the free troposphere. Therefore, the possible role played by emissions occurring in the planetary boundary layer (PBL) of the Kathmandu Valley in influencing the variability in SLCF/P at NCO-P was investigated. BC and O_3 concentrations at NCO-P showed a linear correlation with the modeled PBL height over the Kathmandu urban area, providing evidence that the anthropogenic emissions occurring within the Kathmandu PBL could affect the variability in BC and O_3 at NCO-P. Furthermore, when introducing an additional constraint into the analysis (viz., back-trajectories), we show that on days when air mass transport between the two measurement sites was observed (10% of the period), at least 22% and 16% of BC and O_3 variability at NCO-P can be explained by concurrent variability in SLCF/P over the Kathmandu Valley.

Keywords: Black carbon; Ozone; Comparison; Planetary boundary layer; Himalayas.

INTRODUCTION

Black carbon (BC) and tropospheric ozone (O_3) are two key short-lived climate forcers (SLCF/P, see UNEP and WMO, 2011), with harmful implications for climate change and for global and regional air quality. BC, the primary component of soot, has a global positive radiative effect on climate, since it absorbs solar radiation (Andreae and Ramanathan, 2013; Bond *et al.*, 2013). Another example of positive feedback is BC deposition onto ice and snow, which represents a threat to glaciers by increased melting (Gustafsson and Ramanathan, 2016; Xu *et al.*, 2016). BC has also adverse impacts on the human health, with BC particles depositing in the lungs, entering the blood, and possibly leading to cardiopulmonary and cardiovascular diseases (Highwood and Kinnersley, 2006; Anenberg *et al.*, 2012; Janssen *et al.*, 2012). O_3 is a secondary pollutant, produced via photochemical reactions of its precursors (such as CO, CH_4, NO_x and VOCs). It affects the oxidation capacity of the troposphere (Gauss *et al.*, 2003), and is globally recognized as a powerful greenhouse gas with a warming effect on climate (Hartmann *et al.*, 2013). O_3 also has adverse implications for vegetation, ecosystems, and human health (Fowler *et al.*, 2008; Monks *et al.*, 2015; Sinha *et al.*, 2015; van Zelm *et al.*, 2016).

South Asia is commonly identified as one of the "hot spots" concerning air pollution and climate change (Ramanathan *et al.*, 2007; Seinfeld, 2008; Monks *et al.*, 2009). The area is often affected by the "Atmospheric Brown Cloud (ABC)" phenomenon, i.e., layers of absorbing aerosols and atmospheric pollutants (including BC and O_3) that extend spatially from the Indian Ocean to the Himalayas and vertically upward a few kilometers. ABCs have several

---

implications for air quality, human health, food security, and regional climate (Ramanathan *et al.*, 2007; Gustafsson *et al.*, 2009; Shindell *et al.*, 2012).

Recent studies have shown that air masses from the highly polluted areas in south Asia (e.g., the Indo-Gangetic Plain and the Himalayan foothills) can move to the Himalayas; these air masses tend to be rich in SLCF/P, and the transport is due to the regional and local meteorology, including the mountain-valley breeze systems that characterize these areas (e.g., Bonasoni *et al.*, 2010; Ram *et al.*, 2010; Hyvärinen *et al.*, 2011; Lu *et al.*, 2011; Marinoni *et al.*, 2013; Putero *et al.*, 2014; Lüthi *et al.*, 2015; Kumar *et al.*, 2016; Ojha *et al.*, 2016; Dhungel *et al.*, 2018).

Long-term observational studies and field campaigns have demonstrated that the large amounts of SLCF/P measured at various sites in the Himalayas are strongly influenced by the planetary boundary layer (PBL) dynamics over the Thar Desert, the Indo-Gangetic Plain, and the Himalayan foothills (e.g., Pant *et al.*, 2006; Dumka *et al.*, 2010; Kumar *et al.*, 2010; Cristofanelli *et al.*, 2014; Raatikainen *et al.*, 2014; Dumka *et al.*, 2015), leading to harmful implications for the Himalayan air quality and climate (e.g., Dey and Tripathi, 2008; Ming *et al.*, 2008). In these areas, the high levels of SLCF/P are generated by a variety of sources, i.e., transportation, domestic and industrial emissions, garbage burning, and open fire emissions (related to crop management and forest fires).

However, due to the spatially and/or temporally limited observations, studies aimed at representing the transport of polluted air masses from these "hot spots" to the Himalayas are lacking the simultaneous evaluation of the interannual variability of SLCF/P at different measurement sites, as well as the investigation of the specific role played by anthropogenic and natural emissions in determining the SLCF/P variability in the Himalayan region. In this work we provide the first comparison of BC and O_3 concentrations at two measurement sites in Nepal: Paknajol in the Kathmandu Valley and the Nepal Climate Observatory-Pyramid (NCO-P) in the southern Himalayas. While the Kathmandu Valley is one of the regional urban "hot spots" in terms of air pollution (due to the increasing population and rapid but unplanned urbanization, see Sandholz, 2016), NCO-P is a remote site representative of the background conditions that characterize the southern Himalayas. The two measurement sites are just 150 km apart, with an altitudinal difference of ~3700 m (Fig. 1). Nearly three years of simultaneous BC and O_3 observations at these sites (February 2013–October 2015), which represent a unique dataset in the region, allowed us to investigate the possible role played by the PBL and transport over the Kathmandu Valley (the closest metropolitan area to NCO-P, in the Himalayan foothills), in addition to the effects on SLCF/P variability in the southern Himalayas.

MATERIALS AND METHODS

Measurement Sites and Instrumental Setup

The Nepal Climate Observatory-Pyramid (NCO-P; 27.95°N, 86.82°E, 5079 m a.s.l.) WMO/GAW global station is located at a remote site in the southern Himalayas; more specifically, it lies in the Khumbu Valley of Nepal, near the base camp of Mt. Everest. The site is not influenced by direct anthropogenic sources, however the valley wind thermal regime systematically favors the transport of polluted air masses from the lower troposphere/Himalayan foothills up to the measurement site (Bonasoni *et al.*, 2010). Therefore, the high-altitude NCO-P station is ideal for investigating the impact of regional pollution to the Himalayan environment, as well as for evaluating the role played by the mountain range in the transport and release of pollutants into the free troposphere.

The Paknajol sampling site (27.72°N, 85.30°E, 1380 m a.s.l.) is located in the Kathmandu tourist district of Thamel. It stands on the top of a building (approximately 25 m a.g.l.), having a free 360° horizon with a range of 300 m. As presented in Putero *et al.* (2015), Paknajol observations are representative of the anthropogenic emissions occurring in the Kathmandu Valley, hereby used as a benchmark for the polluted conditions of the Himalayan foothills.

The simultaneous measurements that were made are as follows: surface O_3, using an UV-absorption (λ = 254 nm) analyzer (TEI 49i, Thermo Environmental); equivalent black carbon, hereafter referred to as BC, using a Multi Angle
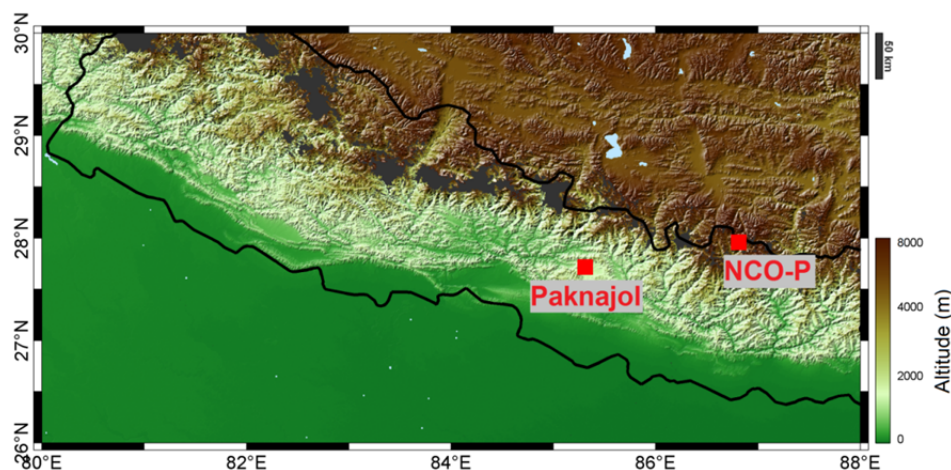

Fig. 1. Geographic map of Nepal with the locations of Paknajol and NCO-P.

Absorption Photometer (MAAP 5012, Thermo Electron Corporation); and meteorological parameters (Weather Transmitter WXT 510, Vaisala). The measurements started at NCO-P in 2006, and at Paknajol in 2013, but were continuously carried out at both sites from February 2013 to October 2015. Further details on the measurement sites and the instrumental setups are given in previous publications (Bonasoni *et al.*, 2010; Cristofanelli *et al.*, 2010; Marinoni *et al.*, 2010; Putero *et al.*, 2015). All data were stored and validated on a 1 min basis, and expressed in STP conditions (0°C and 1013 hPa). They were then averaged to a common time base of 60 min, on the condition that at least 50% of the time interval was covered by data.

Satellite Datasets

CO values used in this work were taken from the Atmospheric InfraRed Sounder (AIRS) onboard the NASA Aqua satellite. The Level-3 daily 1° × 1° gridded standard products (AIRX3STD, see McMillan *et al.*, 2011), were taken for the grid point closest to the coordinates of Paknajol, and at the vertical slice of 850 hPa. To obtain better spatial coverage, as well as to minimize the day/night difference, the daytime/ascending and the nighttime/descending retrievals were averaged to obtain each daily CO value.

Tropospheric NO_2 observations were derived from the OMI/Aura retrievals (Levelt *et al.*, 2006). In particular, we used the Level-3 daily 0.25° × 0.25° globally gridded total and tropospheric NO_2 product (OMNO2d, see Bucsela *et al.*, 2006). Each NO_2 value reported refers to the number of molecules in an atmospheric column extending from the surface to the top of the troposphere. Furthermore, only data were used for which cloud radiance fraction was less than 30%.

Back-Trajectories and PBL Height

To evaluate the synoptic-scale variability of the air masses reaching NCO-P, sets of 5-day back-trajectories were computed every 6 h, starting at this measurement site (starting at 0:00, 6:00, 12:00 and 18:00 UTC); this was done using the Lagrangian analysis tool LAGRANTO (Wernli and Davies, 1997; Sprenger and Wernli, 2015). The back-trajectory calculations are based on the 6-hourly ERA-Interim reanalysis of the ECMWF (European Centre for Medium-Range Weather Forecast, see Dee *et al.* 2011). To partially compensate for uncertainties related to the absence of subgrid scale processes in LAGRANTO (e.g., convection and turbulent diffusion), each set comprised 12 back-trajectories, with starting positions shifted by ±1° in latitude/longitude and in the vertical range of ±50 hPa with respect to the location of NCO-P. The temporal resolution for the back-trajectories was one point every 2 h.

The PBL height over Kathmandu was retrieved from the ERA-Interim reanalysis dataset (Dee *et al.*, 2011), of which the spatial resolution is approximately 80 km (T255 spectral). Since there is no exact value corresponding to Kathmandu coordinates, we obtained it by linearly interpolating the two grid points closest to the location of Paknajol. The temporal resolution for the PBL dataset is one value every 3 h, then used to obtain an average daily value.

As also mentioned by Raatikainen *et al.* (2014), it is well known that both back-trajectory calculations and modeled PBL height suffer from uncertainties in mountainous environments. However, several studies (e.g., Seidel *et al.*, 2012; Leventidou *et al.*, 2013; von Engeln and Teixeira, 2013; Guo *et al.*, 2016) have compared ERA-Interim PBL values to other types of observations in different parts of the world, highlighting that the ERA-Interim values all reproduce spatial, seasonal and diurnal patterns of PBL variability. To check the representativeness of the ERA-Interim PBL values used in this work, we compared the first year of data to the mixing layer height observations measured at Bode, a semi-urban site in the Kathmandu Valley (Mues *et al.*, 2017). Despite some differences concerning the exact position of the maximum, the two time series were in good agreement for what concerns the diurnal averages and the amplitude of the maximum itself (Fig. S1 in the Supplementary Material).

Due to the lack of other continuous direct observations during the period under study in Kathmandu (e.g., radiosondes), we thought it justified to use the ERA-Interim daily PBL averages for linking the day-to-day observations between the two measurement sites.

RESULTS AND DISCUSSION

Transport Patterns

Both measurement sites are affected by a synoptic-scale circulation modulated by the occurrence of the south Asian monsoon. During non-monsoon seasons, due to the influence of the subtropical jet stream, a westerly circulation prevails, with limited vertical displacement of air masses. Conversely, the summer monsoon season is affected by a prevalent southern circulation characterized by the enhanced vertical uplift of air masses from the Indian subcontinent and the Indian Ocean (for more details, see Fig. S2 in the Supplementary Material, and Bonasoni *et al.*, 2010; Balestrini *et al.*, 2016). As also asserted in Putero *et al.* (2015), the seasonal onset and decay dates do not usually differ too much between the two measurement sites. To this aim, they were defined according to the seasonal variability of the relative humidity and diurnal variations in the meridional wind component, as recommended in Bonasoni *et al.* (2010) (Table 1).

Aside from the synoptic-scale meteorology, both measurement sites are affected by local circulation patterns that can modulate the diurnal variability of BC and O_3. In particular, the Kathmandu Valley is almost completely surrounded by mountains with peaks ranging from 2000 to 2800 m a.s.l., giving the valley a characteristic "bowl" shape; hence the evolution of the PBL and pollutant variability are modulated by local meteorology operating within this terrain. As already presented in several papers (Panday and Prinn, 2009; Panday *et al.*, 2009; Putero *et al.*, 2015), the local meteorology of the Kathmandu Valley is characterized by two very different circulation features: afternoon westerly/northwesterly winds that intrude the valley through the western passes, and low speed katabatic winds that descend from the mountain slopes during the night

Table 1. Onset and decay dates of the different seasons selected in this work.

Year	Season	Start day–End day
2013	Pre-monsoon	1 February–12 May 2013
	Monsoon	13 May–6 October 2013
	Post-monsoon	7 October–26 October 2013
2014	Winter	27 October 2013–31 January 2014
	Pre-monsoon	1 February–7 June 2014
	Monsoon	8 June–3 October 2014
	Post-monsoon	4 October–29 October 2014
2015	Winter	30 October 2014–25 February 2015
	Pre-monsoon	26 February–8 June 2015
	Monsoon	9 June–28 September 2015
	Post-monsoon	29 September–28 October 2015

(see Fig. S3 in the Supplementary Material). This defines a return of pollutants from the previous night, affecting BC diurnal variation (as described in Putero *et al.*, 2015). Conversely, NCO-P is affected by the systematic occurrence of mountain-valley winds in two specific directions determined by the valley's topography (S–SW and N–NE, see Bonasoni *et al.*, 2010). In particular, daytime up-valley winds are observed from October to May, while mountain winds prevail during nighttime. In the summer months however, valley winds are also predominant during night, due to the influence of the Indian monsoon (see Bonasoni *et al.*, 2010, and Fig. S4 in the Supplementary Material).

BC and O₃ Variations at Both Stations

Fig. 2 shows the variation of the daily averages for the parameters considered in this study, as introduced in Sect. 2. In addition to this, the seasonal differences in the BC and O_3 concentrations between NCO-P and Paknajol (i.e., ΔBC and ΔO_3), are reported in Table 2. Between the two measurement sites, BC is characterized by values which differ by nearly one order of magnitude (Fig. 2(a) and Table 2), further indicating the very different nature: Paknajol presented an average BC concentration of 10.2 ± 6.4 µg m^{-3} (average value ±1 standard deviation), while the average BC at NCO-P was 0.3 ± 0.4 µg m^{-3}. Also the seasonality is different: Paknajol recorded the highest BC values in winter (17.9 ± 6.4 µg m^{-3}), while at NCO-P the highest concentrations were found in the pre-monsoon (0.6 ± 0.5 µg m^{-3}). This highlights the specific role of meteorology and valley breeze transport in the latter season at NCO-P. Conversely, the highest wintertime values at Paknajol are representative of an increase in emissions from domestic heating, and the occurrence of stable and dry meteorological conditions favoring the accumulation and trapping of pollutants emitted in the Kathmandu basin (Putero *et al.*, 2015). The lowest concentrations were found during the monsoon for both sites (5.4 ± 1.7 µg m^{-3} and 0.1 ± 0.2 µg m^{-3}, for Paknajol and NCO-P, respectively). The different behavior reflects the occurrence of the south Asian monsoon (as presented in Sect. 3.1), which can be explained by the meteorological patterns that characterize the two areas under study, as well as by the emission and accumulation of pollutants on the local and regional scales. All of the BC values reported in this work are in line with previous

publications (e.g., Putero *et al.*, 2014, 2015).

O_3 variations (Fig. 2(b) and Table 2) were slightly different for the two measurement sites: both presented maximum values in the pre-monsoon (36.5 ± 13.1 nmol mol^{-1} and 58.1 ± 9.0 nmol mol^{-1}, for Paknajol and NCO-P, respectively), while minima were recorded in winter at Paknajol (18.8 ± 4.5 nmol mol^{-1}) and during the monsoon at NCO-P (40.1 ± 11.0 nmol mol^{-1}). NCO-P values resulted always higher than Paknajol (on average: 48.4 ± 11.8 nmol mol^{-1} and 27.1 ± 12.1 nmol mol^{-1}, respectively); this is due to an atmospheric "background", which is higher in the free troposphere of the southern Himalayas (far from pollution sources) with respect to the polluted urban area in the Kathmandu Valley. Like BC, O_3 values are also comparable to those shown in previous publications (such as Putero *et al.*, 2014, 2015).

In addition to the SLCF/P variability, two satellite datasets were analyzed, i.e., CO values from AIRS, and tropospheric NO_2 from OMI (as introduced in Sect. 2.2). CO values (Fig. 2(c)) exhibited a clear seasonal cycle, being the highest in the pre-monsoon (142.2 ± 13.7 nmol mol^{-1}) and the lowest during the monsoon and post-monsoon seasons (119.0 ± 10.9 nmol mol^{-1} and 113.5 ± 10.1 nmol mol^{-1}, respectively). These CO values are lower than previous investigations in the Kathmandu Valley (e.g., Panday and Prinn, 2009; Rupakheti *et al.*, 2017); this is most likely because they refer to an area wider than the Kathmandu urban area itself, and thus include rural zones likely characterized by lower CO emissions. Nonetheless, being the Kathmandu Valley the major source of emissions of the pixel under study, and due to the lack of continuous in situ CO observations for the period of interest, we hereby consider the CO values by AIRS to be representative of the Kathmandu extended urban area. Despite that most of the CO in this area is produced by anthropogenic emissions (e.g., traffic, domestic heating, combustion of fossil fuels in industries), a non-negligible part derives from waste and biomass burning (Stockwell *et al.*, 2016; Rupakheti *et al.*, 2017). To better highlight the mutual variations along with CO, Fig. 2(c) shows the number of fires observed by MODIS (MCD14ML product, see Justice *et al.*, 2002) in a $2° \times 2°$ area around the location of Paknajol (i.e., 27–29°N, 84–86°E). From a qualitative point of view, it is worth noting the co-variability between CO and the number of fires; the events characterized by increased fire emissions correspond to high CO levels
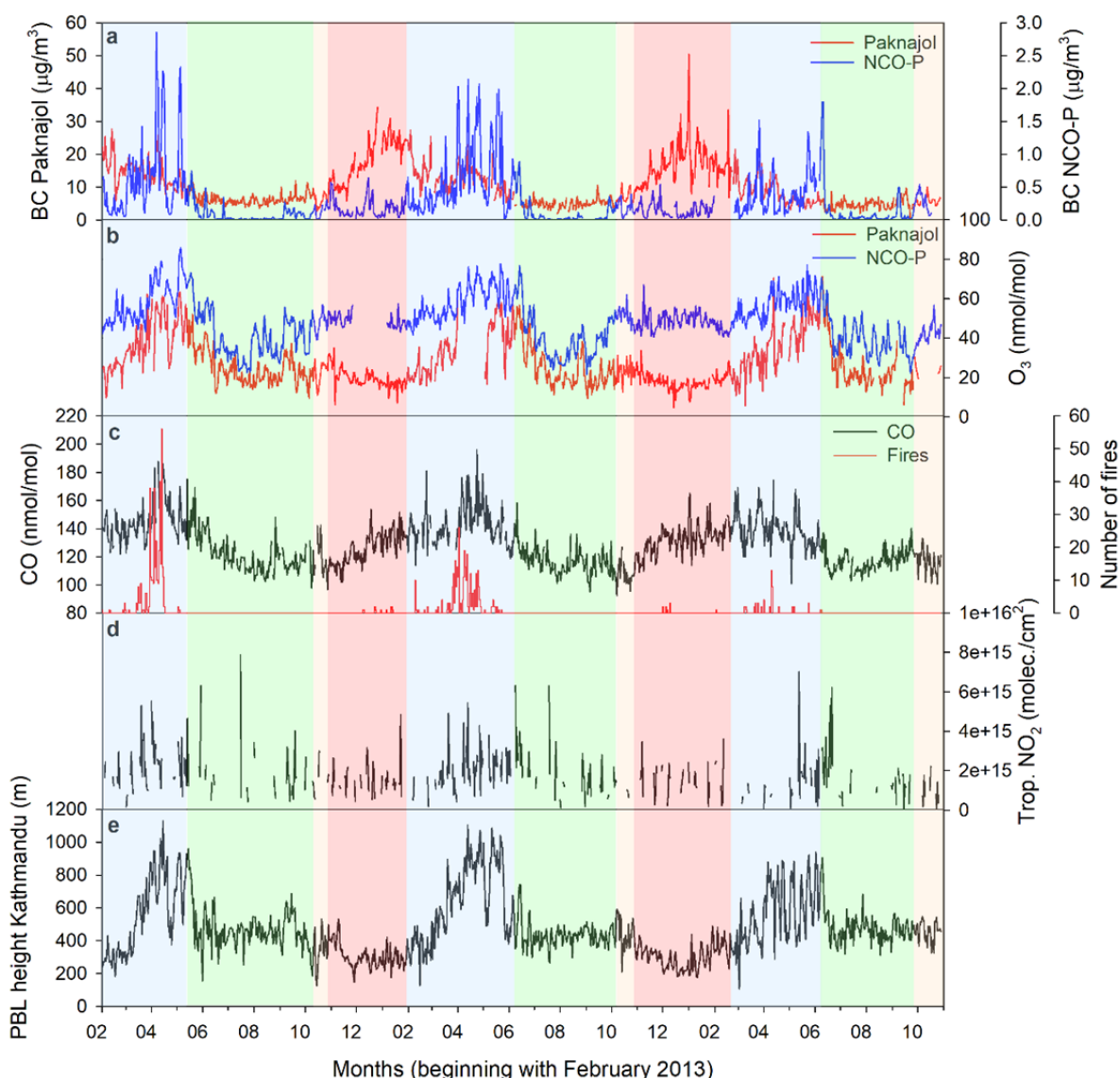
Fig. 2. Time series of daily values for black carbon (BC, panel a) and surface ozone (O₃, panel b) at both Paknajol (red line) and NCO-P (blue line) stations, CO (c), tropospheric NO₂ column (d), and planetary boundary layer (PBL) height over an area that comprises Kathmandu (e). Together with CO (c) is shown the number of fires observed by MODIS in a 2° × 2° area enclosing the Kathmandu Valley (i.e., 27–29°N, 84–86°E). Shaded areas in the figure indicate the different seasons, as reported in Table 1 (blue: pre-monsoon, green: monsoon, orange: post-monsoon and red: winter).

Table 2. Seasonal ΔBC and ΔO₃ values, i.e., the difference between NCO-P and Paknajol concentrations.

Season	ΔBC ($\mu g\ m^{-3}$)	ΔO₃ ($nmol\ mol^{-1}$)
Pre-monsoon	−11.3	21.6
Monsoon	−5.3	15.2
Post-monsoon	−6.2	23.6
Winter	−17.4	29.7

(e.g., March 30th–April 16th, 2013, and March 29th–April 28th, 2014). Similarly, when lower than usual fire activity was observed, CO mixing did not exhibit the distinct annual peak (i.e., winter and pre-monsoon 2015).

Variations in the tropospheric NO₂ column (hereinafter referred to as NO₂, for simplicity), over the grid point related to the Kathmandu Valley, are shown in Fig. 2(d).

NO₂ is used since it is a photochemical precursor of O₃, being formed by combustion processes related to vehicular traffic or biomass burning. Although several gaps in the time series were present throughout the period under study, the NO₂ variations at Kathmandu followed a seasonality similar to that of CO: the highest values were found in the pre-monsoon ($1.9 \pm 1.2 \times 10^{15}$ molec. cm^{-2}), favored by low

humidity and mild temperatures that cause reduction in the photolysis removal processes of NO_2, and the lowest in the post-monsoon ($1.2 \pm 0.6 \times 10^{15}$ molec. cm^{-2}). These results appear higher than the tropospheric NO_2 values reported in a trend study computed over the last decade (i.e., $1.03 \pm 0.05 \times 10^{15}$ molec. cm^{-2}, see ul-Haq *et al.*, 2015), and consistent with the increasing trends that were found to characterize the tropospheric NO_2 concentrations in both Nepal and in south Asia (Ghude *et al.*, 2009; ul-Haq *et al.*, 2015).

### Effects of PBL Variability on BC and O₃ Concentrations at NCO-P

The possible role of PBL variability over the Himalayan foothills in favoring the transport of polluted air masses rich in BC and O_3 was investigated. We analyzed the BC and O_3 variability at NCO-P as a function of the PBL height over a pixel that enclosed the Kathmandu urban area. A similar approach was proposed by Raatikainen *et al.* (2014), who showed that the aerosol concentrations measured in the western Himalayan foothills were correlated with the spatially-averaged PBL height over the Indo-Gangetic Plain. Carrying out a similar analysis for NCO-P is important for extending the findings by Raatikainen *et al.* (2014) to a broader Himalayan region.

Fig. 3 shows the scatter plot of daily average BC (panel a) and O_3 (panel b) concentrations at NCO-P versus PBL height over the Kathmandu urban area (as presented in Sect. 2.3). Colors in the plot indicate the different seasons, as defined in Sect. 3.1. Both parameters showed statistically significant ($p < 0.05$) linear correlation with the PBL height over Kathmandu ($r^2 = 0.35$ for BC, and $r^2 = 0.26$ for O_3, respectively), suggesting that the latter can be an important parameter explaining the transport and SLCF/P variability at NCO-P. The linear correlation was also maintained

when each season was investigated separately. For BC, the seasonally-divided correlation is shown in Fig. 4, where colors indicate the CO values representative of the Kathmandu urban area (see Sect. 2.2). The analysis for the post-monsoon is not as robust as in the other seasons due to lower data availability; therefore it will not be discussed here. The correlation remained statistically significant during pre-monsoon and monsoon ($r^2 = 0.27$ for both seasons), with the highest BC values observed together with the highest CO retrievals (see also Fig. S5 in the Supplementary Material). This suggests that the combustion processes occurring over the Kathmandu region can contribute, under favorable PBL conditions, in modulating BC variability at NCO-P. Similarly, seasonal O_3 correlations with PBL variations are shown in Fig. 5. Colors in this plot denote the NO_2 values over Kathmandu retrieved by OMI (see Sect. 2.2). Unlike BC, the correlation coefficients were statistically significant only during pre-monsoon and monsoon ($r^2 = 0.44$ and $r^2 = 0.20$, respectively). Although the NO_2 levels showed large variability within each season (see Fig. 2(d)), the high NO_2 associated with high O_3 mixing ratios at NCO-P (see Fig. S6 in the Supplementary Material) indicated the possibility that anthropogenic emissions occurring at Kathmandu could affect, after photochemical production and transport, the O_3 variability at NCO-P.

The interannual variability of r^2 between PBL height and BC and O_3 concentrations was further examined (Table 3). Compared to other years, the r^2 values were lower for both species in 2015; in addition, no significant differences were observed in the local and regional meteorology with respect to the rest of the investigated period (i.e., variations in the transport patterns or in the precipitation at NCO-P). As presented in Table 3, this behavior, which is linked to a decrease in the BC and O_3 concentrations for relatively high
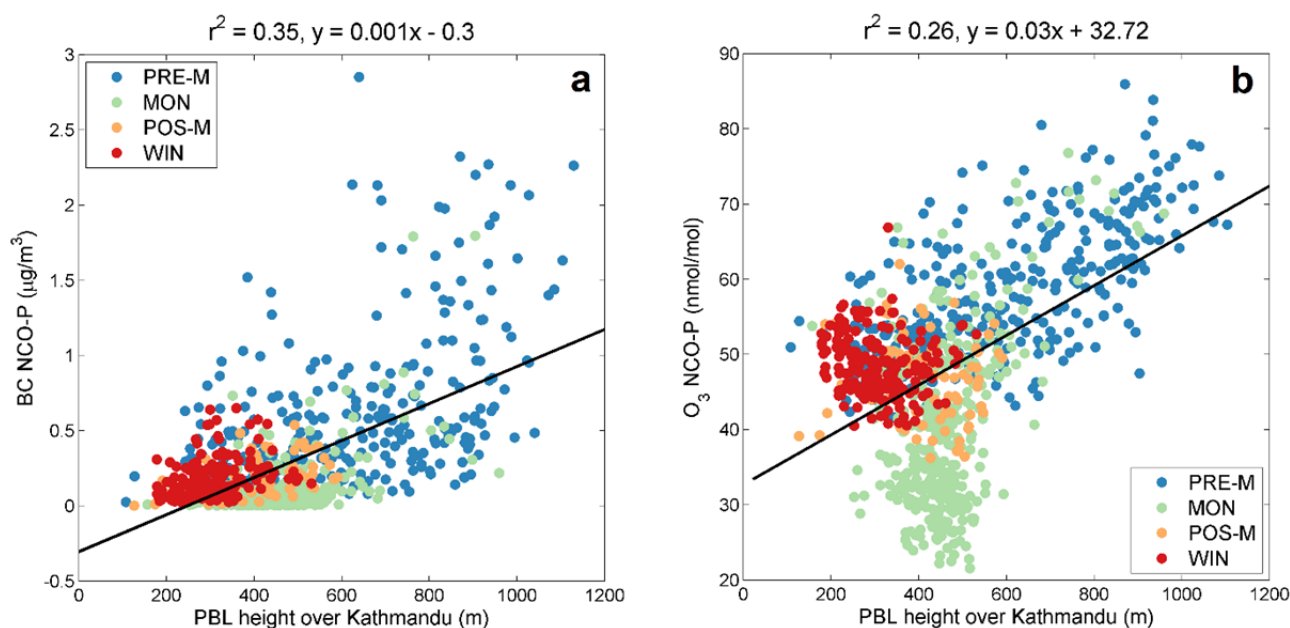
Fig. 3. Scatter plots of daily average BC (a) and O_3 (b) concentrations at NCO-P, as a function of the PBL height over Kathmandu. Colors indicate the different seasons (PRE-M: pre-monsoon, MON: monsoon, POS-M: post-monsoon, and WIN: winter). The linear fits considering the entire dataset are also reported in the plot.
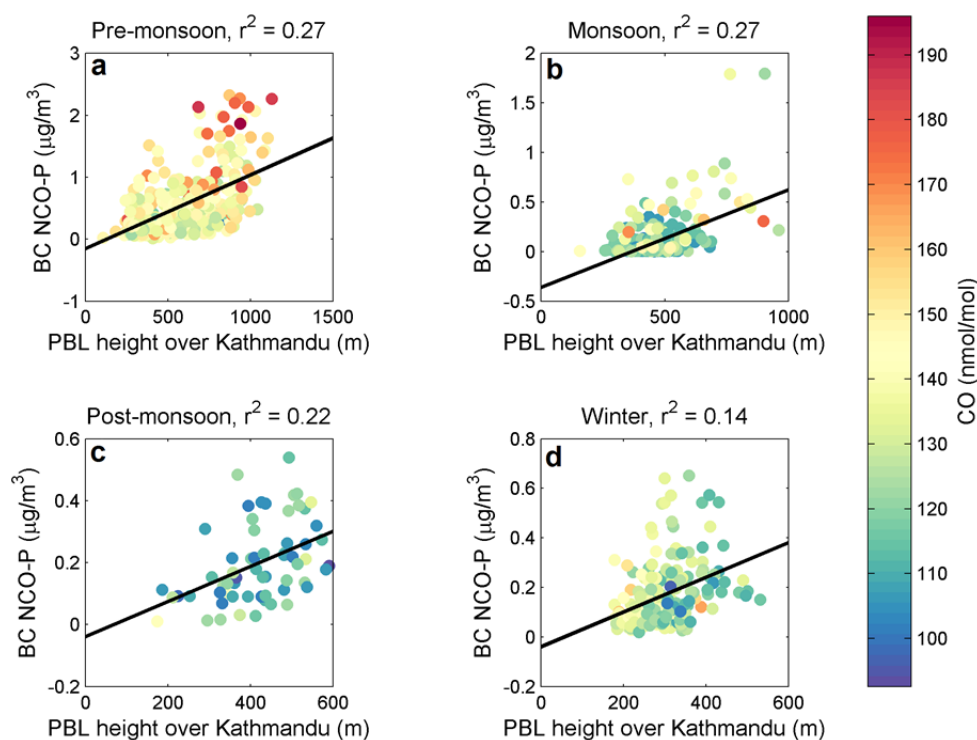
Fig. 4. Seasonal scatter plots of daily average BC concentrations at NCO-P, as a function of the PBL height over Kathmandu. Colors indicate the CO value over a region including Kathmandu, as retrieved by AIRS. The linear fits are also reported in each plot.
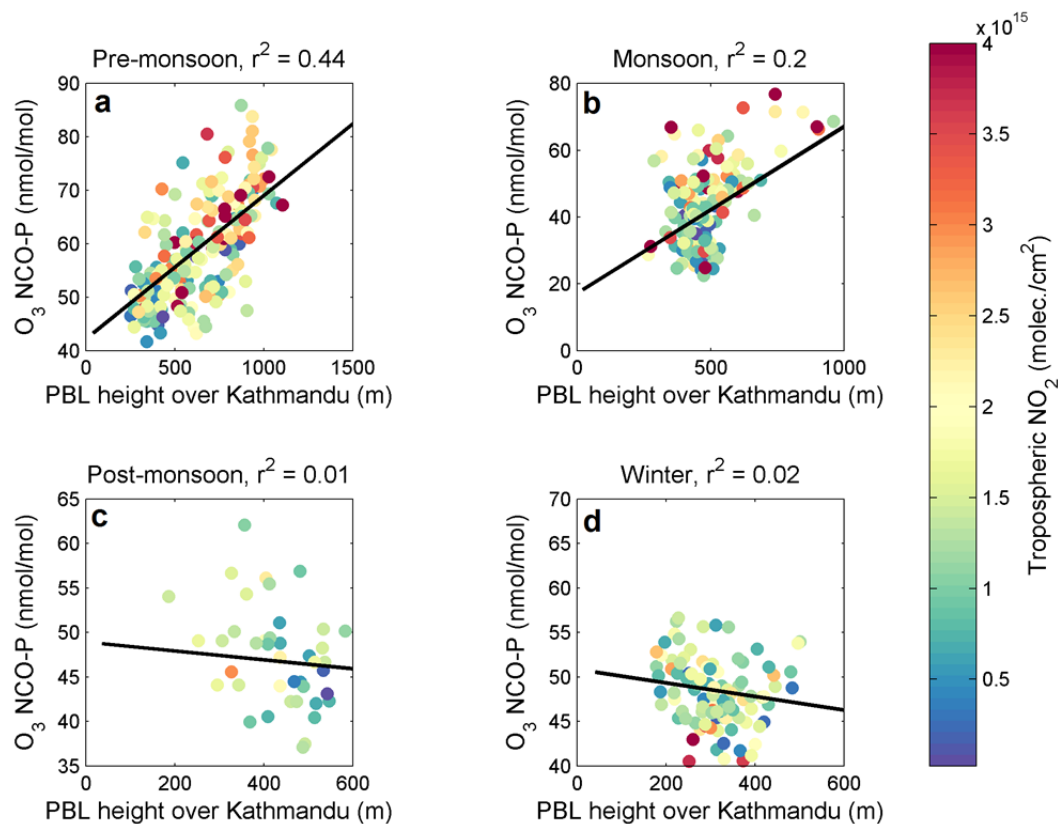
Fig. 5. Seasonal scatter plots of daily average O_3 concentrations at NCO-P, as a function of the PBL height over Kathmandu. Colors indicate the tropospheric NO_2 column over Kathmandu, as retrieved by OMI. The linear fits are also reported in each plot.

Table 3. Correlation coefficients (r^2) between PBL heights over Kathmandu and BC and O_3 concentrations at NCO-P, for the years considered in this study. Also reported in the Table are the number of days (i.e., n), as well as the number of fires observed by MODIS in a $2° \times 2°$ area enclosing the Kathmandu Valley (i.e., 27–29°N, 84–86°E).

| Year	BC	O_3	n	Fires (#)
2013	0.29	0.31	268	394
2014	0.51	0.34	368	321
2015	0.20	0.13	364	62
All	0.35	0.26	1000	777

(i.e., > 800 m) PBL values, can be attributed to lower fire emissions: 2015 registered a significant reduction in the number of fires observed by MODIS in the region of interest (–81%, and –84% with respect to the total fire counts in 2014 and 2013, respectively).

To provide further evidence of the role played by the transport of polluted air masses from Kathmandu towards NCO-P, we considered back-trajectories as a constraint in the correlation analysis. More specifically, the analysis was restricted only to days characterized by the presence of at least 3% of daily back-trajectories from NCO-P that have crossed the PBL over Kathmandu. This was performed by checking if each back-trajectory crossed an idealized 3-dimensional cell of $0.5° \times 0.5°$ containing Paknajol at its center, and whose vertical dimension was given by the PBL height value. Since the temporal resolution for the back-trajectories is 2 h, at each point the altitude field was compared to the PBL height closest in time, thus resulting in a possible minor source of uncertainty. After performing a sensitivity study, we chose the value of 3% to partially compensate for such uncertainties, as well as to give a robust identification of the possible transport.

Concerning the transport times, the frequency distribution of Δt (i.e., the time between the crossing of the PBL over

Kathmandu and the arrival of the same air mass at NCO-P) showed that more than one-third (47%) of the data had values lower than one day, and that 74% of the travel times were enclosed within 48 h (Fig. 6). This is consistent with the results presented in Lüthi *et al.* (2015), indicating that relatively "fast" transport characterizes the travel of air masses from the Indo-Gangetic Plain/Himalayan foothills to the Himalayas.

Fig. 7 shows the BC and O_3 concentrations at NCO-P as a function of the PBL height variations at Kathmandu on this subset of days only. To better estimate the correct transport times for each *x*-th day, each BC and O_3 daily average at NCO-P was associated with the corresponding $(x + \overline{\Delta t})$ PBL height daily value, where $\overline{\Delta t}$ represents the median of the Δt values computed on each *x*-th day. Similarly, colors in the plots denote the BC and O_3 $(x + \overline{\Delta t})$ daily averages recorded at Paknajol. The value of the correlation coefficient between the PBL height and BC at NCO-P increased from $r^2 = 0.35$ to $r^2 = 0.47$. The same behavior was observed for O_3, with an increase in the correlation coefficient from $r^2 = 0.26$ to $r^2 = 0.52$. Conversely, on days not characterized by back-trajectories crossing the PBL, the linear correlation was comparable to that characterizing the entire period under study, as displayed in Fig. 3 ($r^2 = 0.35$ and $r^2 = 0.25$ for BC and O_3, respectively). Besides, on average, the highest BC and O_3 concentrations at NCO-P corresponded to the highest concentrations measured at Paknajol. This was also observable from the statistically significant correlations (Fig. S7 in the Supplementary Material) between these parameters ($r^2 = 0.28$ and $r^2 = 0.60$ for BC and O_3, respectively), which were higher on this subset of days, with respect to the correlations characterizing the entire period of study ($r^2 = 0.06$ and $r^2 = 0.44$ for BC and O_3, respectively). It is worth noting that two of the points characterized by very high BC values at NCO-P (Fig. 7(a)) correspond to the day (and the following ones) on which the Nepali new year was celebrated in Kathmandu (i.e.,
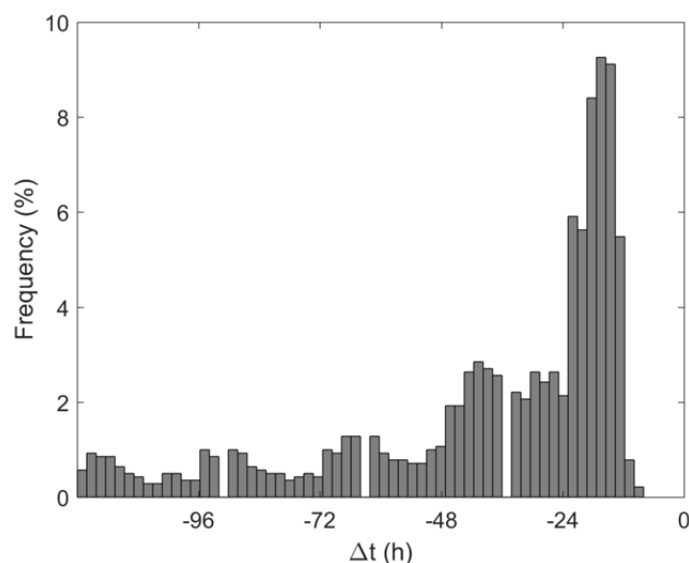
Fig. 6. Distribution of Δt, i.e., the time difference (in hours) between the crossing of the PBL over Kathmandu and the arrival of the same air-mass at NCO-P.
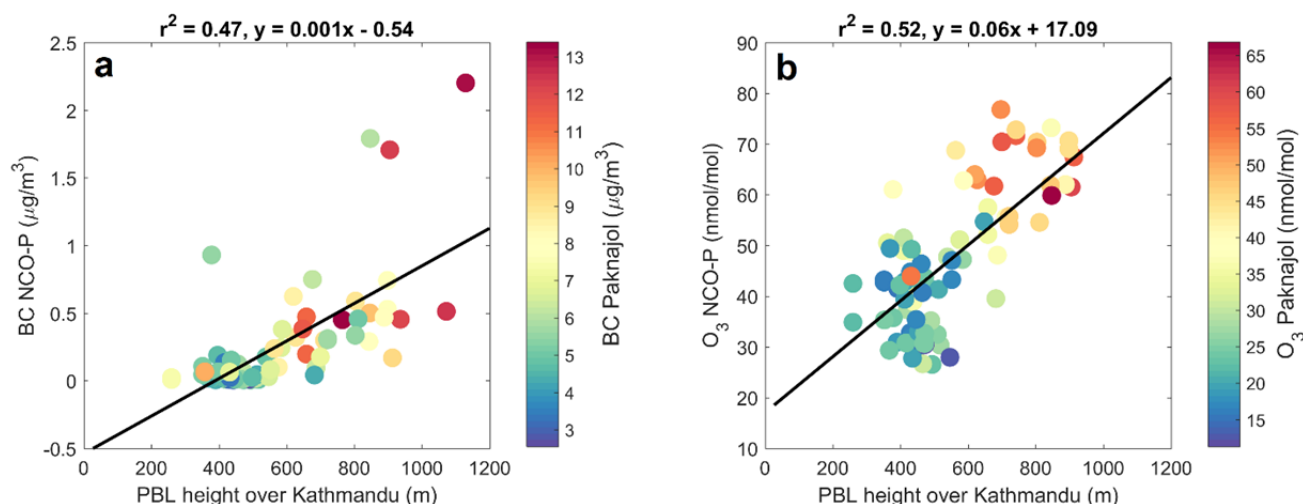
Fig. 7. Scatter plots of daily average BC (a) and O_3 (b) concentrations at NCO-P, as a function of the PBL height over Kathmandu. Colors indicate the BC (a) and O_3 (b) daily values recorded at Paknajol. Displayed are only the days on which at least 3% of back-trajectories starting at NCO-P have crossed the PBL over Kathmandu; moreover, for each day the median Δt value was taken into account (as described in Sect. 3.3). The linear fits are also reported in each plot.

April 14th, 2013). Indeed, in addition to the regular activities, increased emissions due to celebrations (e.g., parades, festivals) can be observed at Kathmandu during these days. Under favorable transport conditions, these air masses enriched in combustion by-products can travel up to the Himalayas and be detected at NCO-P.

CONCLUSIONS

In this work, we reported nearly 3 years (February 2013–October 2015) of continuous BC and O_3 measurements at two sites in Nepal (viz., Paknajol, in the Kathmandu Valley, and the Nepal Climate Observatory-Pyramid, in the southern Himalayas); specifically, we investigated the role of the PBL and air-mass transport in affecting the variability in SLCF/P over the southern Himalayas.

The two measurement sites are characterized by very different features: Paknajol is considered representative of the anthropogenic emissions that contribute to the poor air quality typical of the Kathmandu Valley, and NCO-P is a remote site representative of the southern-Himalayan free troposphere. The BC and O_3 variations at both sites are naturally driven by regional meteorology and local circulation systems (viz., day/night wind variations).

We conducted a correlation study between the daily PBL height (derived from ERA-Interim), over a pixel that enclosed the Kathmandu urban area, and the daily BC and O_3 concentrations at NCO-P. The parameters showed statistically significant ($p < 0.05$) linear correlations ($r^2 = 0.35$ for BC and $r^2 = 0.26$ for O_3), which were maintained also within each season (all seasons for BC and pre-monsoon and monsoon seasons for O_3). Thus, the PBL height over the Himalayan foothills can be identified as an important parameter in explaining the BC and O_3 variability at NCO-P. To provide a further indication of the role played by transport, we included back trajectories starting at NCO-P as another constraint in the analysis. This constraint led to

the identification of a subset of days (10% of the dataset) characterized by air masses crossing the PBL over the Kathmandu urban area and then arriving at NCO-P. On these days, we observed an increase in the correlation coefficients between the PBL height, and BC and O_3 concentrations at NCO-P ($r^2 = 0.47$ and $r^2 = 0.52$ for BC and O_3, respectively). Conversely, when transport was not observed, a decrease in the r^2 was detected for both parameters. During these days, the highest BC and O_3 values at NCO-P corresponded (on average) to the highest BC and O_3 concentrations measured at Paknajol. Also, the linear-correlation coefficient between BC and O_3 at the two measurement sites increased with respect to the entire study period (r^2 increased from 0.06 to 0.28 for BC and from 0.44 to 0.60 for O_3). This would suggest that when air masses pass through the PBL over Kathmandu, BC and O_3 variability at Paknajol can explain at least 22% and 16% of the variability in BC and O_3, respectively, at NCO-P.

Several limitations of this study must be taken into account, viz., the use of back trajectories in complex mountainous environments, the coarse resolution of satellite/modeled datasets, and the lack of continuous in-situ observations for PBL, CO, and NO_2. With the currently deployed setup, we were unable to identify the sources of the air masses considered and to apportion and quantify the contribution from other polluted areas outside the Kathmandu Valley, e.g., the Indo-Gangetic Plain or the Himalayan foothills, which were categorized in previous works as important source regions for BC and O_3 at NCO-P (e.g., Bonasoni *et al.*, 2010; Cristofanelli *et al.*, 2014; Putero *et al.*, 2014). These topics would certainly be important improvements for future studies, which might include additional measurements in the Indo-Gangetic Plain or other areas in the Himalayan foothills, high-resolution modeling outputs, or the use of specific tracers. Despite these limitations, the consequences of the transport of such harmful air pollutants from a regional "hot spot" to a remote region in

the Himalayas appear evident: Once in the free troposphere, these SLCF/P can increase their lifetimes (with respect to those typical within the PBL) and be transported far from their sources, with potential impacts on the regional and global climate.

ACKNOWLEDGMENTS

SUPPLEMENTARY MATERIAL

Supplementary data associated with this article can be found in the online version at http://www.aaqr.org.

REFERENCES

Andreae, M.O. and Ramanathan, V. (2013). Climate's dark forcings. *Science* 340: 280–281.

Anenberg, S.C., Schwartz, J., Shindell, D., Amann, M., Faluvegi, G., Klimont, Z., Janssens-Maenhout, G., Pozzoli, L., Van Dingenen, R., Vignati, E., Emberson, L., Muller, N.Z., West, J.J., Williams, M., Demkine, V., Hicks,W. K., Kuylestierna, J., Reas, F. and Ramanathan, V. (2012). Global air quality and health co-benefits of mitigating near-term climate change through methane and black carbon emission controls. *Environ. Health Perspect.* 120: 831–839.

Balestrini, R., Delconte, C.A., Sacchi, E., Wilson, A.M., Williams, M.W., Cristofanelli, P. and Putero, D. (2016). Wet deposition at the base of Mt Everest: Seasonal evolution of the chemistry and isotopic composition. *Atmos. Environ.* 146: 100−112.

Bonasoni, P., Laj, P., Marinoni, A., Sprenger, M., Angelini, F., Arduini, J., Bonafe, U., Calzolari, F., Colombo, T., Decesari, S., Di Biagio, C., di Sarra, A. G., Evangelisti, F., Duchi, R., Facchini, M., Fuzzi, S., Gobbi, G. P., Maione, M., Panday, A., Roccato, F., Sellegri, K., Venzac, H., Verza, G., Villani, P., Vuillermoz, E. and Cristofanelli, P. (2010). Atmospheric Brown Clouds in the Himalayas: First two years of continuous observations at the Nepal Climate Observatory-Pyramid (5079 m). *Atmos. Chem. Phys.* 10: 7515–7531.

Bond, T.C., Doherty, S.J., Fahey, D.W., Forster, P.M., Berntsen, T., DeAngelo, B.J., Flanner, M.G., Ghan, S., Kärcher, B., Koch, D., Kinne, S., Kondo, Y., Quinn, P. K., Sarofim, M.C., Schultz, M.G., Schulz, M., Venkataraman, C., Zhang, H., Zhang, S., Bellouin, N., Guttikunda, S. K., Hopke, P.K., Jacobson, M.Z., Kaiser, J.W., Klimont, Z., Lohmann, U., Schwarz, J.P., Shindell, D., Storelvmo, T., Warren, S.G. and Zender, C.S. (2013). Bounding the role of black carbon in the climate system: A scientific assessment. *J. Geophys. Res.* 118: 5380–5552.

Bucsela, E.J., Celarier, E.A., Wenig, M.O., Gleason, J.F., Veefkind, J.P., Boersma, K.F. and Brinksma, E.J. (2006). Algorithm for NO_2 vertical column retrieval from the ozone monitoring instrument. *IEEE Trans. Geosci. Remote Sens.* 44: 1245–1258.

Cristofanelli, P., Bracci, A., Sprenger, M., Marinoni, A., Bonafè, U., Calzolari, F., Duchi, R., Laj, P., Pichon, J., Roccato, F., Venzac, H., Vuillermoz, E. and Bonasoni, P. (2010). Tropospheric ozone variations at the Nepal Climate Observatory-Pyramid (Himalayas, 5079 m asl) and influence of deep stratospheric intrusion events. *Atmos. Chem. Phys.* 10: 6537–6549.

Cristofanelli, P., Putero, D., Adhikary, B., Landi, T., Marinoni, A., Duchi, R., Calzolari, F., Laj, P., Stocchi, P., Verza, G., Vuillermoz, E., Kang, S., Ming, J. and Bonasoni, P. (2014). Transport of short-lived climate forcers/pollutants (SLCF/P) to the Himalayas during the South Asian summer monsoon onset. *Environ. Res. Lett.* 9: 084005.

Dee, D.P., Uppala, S.M., Simmons, A.J., Berrisford, P., Poli, P., Kobayashi, S., Andrae, U., Balmaseda, M.A., Balsamo, G., Bauer, P., Bechtold, P., Beljaars, A.C.M., van de Berg, L., Bidlot, J., Bormann, N., Delsol, C., Dragani, R., Fuentes, M., Geer, A.J., Haimberger, L., Healy, S.B., Hersbach, H., Hólm, E.V., Isaksen, L., Kållberg, P., Köhler, M., Matricardi, M., McNally, A. P., Monge-Sanz, B.M., Morcrette, J.J., Park, B.K., Peubey, C., de Rosnay, P., Tavolato, C., Thépaut, J.N. and Vitart, F. (2011). The ERA-Interim reanalysis: Configuration and performance of the data assimilation system. *Q. J. R. Meteorolog. Soc.* 137: 553–597.

Dey, S. and Tripathi, S.N. (2008). Aerosol direct radiative effects over Kanpur in the Indo-Gangetic basin, northern India: Long-term (2001–2005) observations and implications to regional climate. *J. Geophys. Res.* 113: D04212.

Dhungel, S., Kathayat, B., Mahata, K. and Panday, A. (2018). Transport of regional pollutants through a remote trans-Himalayan valley in Nepal. *Atmos. Chem. Phys. Discuss.* 18: 1203–1216.

Dumka, U.C., Moorthy, K.K., Kumar, R., Hegde, P., Sagar, R., Pant, P., Singh, N. and Babu, S.S. (2010). Characteristics of aerosol black carbon mass concentration over a high altitude location in Central Himalayas from multi-year measurements. *Atmos. Res.* 96: 510–521.

Dumka, U.C., Kaskaoutis, D.G., Srivastava, M.K. and Devara, P.C.S. (2015). Scattering and absorption properties of near-surface aerosol over Gangetic–Himalayan region: The role of boundary-layer dynamics and long-range transport. *Atmos. Chem. Phys.* 15: 1555–1572.

Fowler, D., Amann, M., Anderson, R., Ashmore, M., Cox, P., Depledge, M., Derwent, D., Grennfelt, P., Hewitt, N.,

Hov, O., Jenkin, M., Kelly, F., Liss, P., Pilling, M., Pyle, J., Slingo, J. and Stevenson, D. (2008). *Ground-level ozone in the 21st century: Future trends, impacts and policy implications.* Vol. 15/08 of Royal Society Policy Document 15/08. The Royal Society, RS1276 Edn.

Gauss, M., Myhre, G., Pitari, G., Prather, M.J., Isaksen, I.S.A., Berntsen, T.K., Brasseur, G.P., Dentener, F.J., Derwent, R.G., Hauglustaine, D.A., Horowitz, L.W., Jacob, D.J., Johnson, M., Law, K.S., Mickley, L.J., Müller, J.F., Plantevin, P.H., Pyle, J.A., Rogers, H.L., Stevenson, D.S., Sundet, J.K., van Weele, M. and Wild, O. (2003). Radiative forcing in the 21st century due to ozone changes in the troposphere and the lower stratosphere. *J. Geophys. Res.* 108: 4292.

Ghude, S.D., van der A, R., Beig, G., Fadnavis, S. and Polade, S. (2009). Satellite derived trends in NO_2 over the major global hotspot regions during the past decade and their inter-comparison. *Environ. Pollut.* 157: 1873–1878.

Guo, J., Miao, Y., Zhang, Y., Liu, H., Li, Z., Zhang, W., He, J., Lou, M., Yan, Y., Bian, L. and Zhai, P. (2016). The climatology of planetary boundary layer height in China derived from radiosonde and reanalysis data. *Atmos. Chem. Phys.* 16: 13309–13319.

Gustafsson, Ö., Kruså, M., Zencak, Z., Sheesley, R.J., Granat, L., Engström, E., Praveen, P., Rao, P., Leck, C. and Rodhe, H. (2009). Brown clouds over south Asia: Biomass or fossil fuel combustion? *Science* 323: 495–498.

Gustafsson, Ö. and Ramanathan, V. (2016). Convergence on climate warming by black carbon aerosols. *Proc. Natl. Acad. Sci. U.S.A.* 113: 4243–4245.

Hartmann, D., Klein Tank, A., Rusticucci, M., Alexander, L., Bronnimann, S., Charabi, Y., Dentener, F., Dlugokencky, E., Easterling, D., Kaplan, A., Soden, B., Thorne, P., Wild, M. and Zhai, P. (2013). Observations: Atmosphere and Surface. In *Climate Change 2013: The Physical Science Basis.* Contribution of Working Group I to the Fifth Assessment Report of the Intergovernmental Panel on Climate Change. Cambridge University Press, Cambridge, United Kingdom and New York, NY, USA.

Highwood, E.J. and Kinnersley, R.P. (2006). When smoke gets in our eyes: The multiple impacts of atmospheric black carbon on climate, air quality and health. *Environ. Int.* 32: 560–566.

Hyvärinen, A.P., Raatikainen, T., Brus, D., Komppula, M., Panwar, T.S., Hooda, R.K., Sharma, V.P. and Lihavainen, H. (2011). Effect of the summer monsoon on aerosols at two measurement stations in Northern India part 1: PM and BC concentrations. *Atmos. Chem. Phys.* 11: 8271–8282.

Janssen, N.A., Gerlofs-Nijland, M.E., Lanki, T., Salonen, R.O., Cassee, F., Hoek, G., Fischer, P., Brunekreef, B. and Krzyzanowski, M. (2012). *Health effects of black carbon.* WHO Regional Office for Europe, Copenhagen.

Justice, C., Giglio, L., Korontzi, S., Owens, J., Morisette, J., Roy, D., Descloitres, J., Alleaume, S., Petitcolin, F. and Kaufman, Y. (2002). The MODIS fire products. *Rem. Sens. Environ.* 83: 244–262.

Kumar, A., Ram, K. and Ojha, N. (2016). Variations in carbonaceous species at a high-altitude site in western India: Role of synoptic scale transport. *Atmos. Environ.* 125: 371–382.

Kumar, R., Naja, M., Venkataramani, S. and Wild, O. (2010). Variations in surface ozone at Nainital: A high-altitude site in the central Himalayas. *J. Geophys. Res.* 115: D16302.

Levelt, P.F., van den Oord, G.H., Dobber, M.R., Malkki, A., Visser, H., de Vries, J., Stammes, P., Lundell, J.O. and Saari, H. (2006). The Ozone Monitoring Instrument. *IEEE Trans. Geosci. Remote Sens.* 44: 1093–1101.

Leventidou, E., Zanis, P., Balis, D., Giannakaki, E., Pytharoulis, I. and Amiridis, V. (2013). Factors affecting the comparisons of planetary boundary layer height retrievals from CALIPSO, ECMWF and radiosondes over Thessaloniki, Greece. *Atmos. Environ.* 74: 360–366.

Lu, Z., Zhang, Q. and Streets, D.G. (2011). Sulfur dioxide and primary carbonaceous aerosol emissions in China and India, 1996–2010. *Atmos. Chem. Phys.* 11: 9839–9864.

Lüthi, Z.L., Škerlak, B., Kim, S.W., Lauer, A., Mues, A., Rupakheti, M. and Kang, S. (2015). Atmospheric brown clouds reach the Tibetan Plateau by crossing the Himalayas. *Atmos. Chem. Phys.* 15: 6007–6021.

Marinoni, A., Cristofanelli, P., Laj, P., Duchi, R., Calzolari, F., Decesari, S., Sellegri, K., Vuillermoz, E., Verza, G., Villani, P. and Bonasoni, P. (2010). Aerosol mass and black carbon concentrations, a two year record at NCO-P (5079 m, Southern Himalayas). *Atmos. Chem. Phys.* 10: 8551–8562.

Marinoni, A., Cristofanelli, P., Laj, P., Duchi, R., Putero, D., Calzolari, F., Landi, T.C., Vuillermoz, E., Maione, M. and Bonasoni, P. (2013). High black carbon and ozone concentrations during pollution transport in the Himalayas: Five years of continuous observations at NCO-P global GAW station. *J. Environ. Sci.* 25: 1618–1625.

McMillan, W.W., Evans, K.D., Barnet, C.D., Maddy, E.S., Sachse, G.W. and Diskin, G.S. (2011). Validating the AIRS Version 5 CO retrieval with DACOM in situ measurements during INTEX-A and-B. *IEEE Trans. Geosci. Remote Sens.* 49: 2802–2813.

Ming, J., Cachier, H., Xiao, C., Qin, D., Kang, S., Hou, S. and Xu, J. (2008). Black carbon record based on a shallow Himalayan ice core and its climatic implications. *Atmos. Chem. Phys.* 8: 1343–1352.

Monks, P., Granier, C., Fuzzi, S., Stohl, A., Williams, M., Akimoto, H., Amann, M., Baklanov, A., Baltensperger, U., Bey, I., Blake, N., Blake, R., Carslaw, K., Cooper, O., Dentener, F., Fowler, D., Fragkou, E., Frost, G., Generoso, S., Ginoux, P., Grewe, V., Guenther, A., Hansson, H., Henne, S., Hjorth, J., Hofzumahaus, A., Huntrieser, H., Isaksen, I., Jenkin, M., Kaiser, J., Kanakidou, M., Klimont, Z., Kulmala, M., Laj, P., Lawrence, M., Lee, J., Liousse, C., Maione, M., McFiggans, G., Metzger, A., Mieville, A., Moussiopoulos, N., Orlando, J., O'Dowd, C., Palmer, P., Parrish, D., Petzold, A., Platt, U., Pschl, U., Prvt, A., Reeves, C.,

Reimann, S., Rudich, Y., Sellegri, K., Steinbrecher, R., Simpson, D., ten Brink, H., Theloke, J., van der Werf, G., Vautard, R., Vestreng, V., Vlachokostas, C. and von Glasow, R. (2009). Atmospheric composition change – global and regional air quality. *Atmos. Environ.* 43: 5268–5350.

Monks, P.S., Archibald, A.T., Colette, A., Cooper, O., Coyle, M., Derwent, R., Fowler, D., Granier, C., Law, K.S., Mills, G.E., Stevenson, D.S., Tarasova, O., Thouret, V., von Schneidemesser, E., Sommariva, R., Wild, O. and Williams, M.L. (2015). Tropospheric ozone and its precursors from the urban to the global scale from air quality to short-lived climate forcer. *Atmos. Chem. Phys.* 15: 8889–8973.

Mues, A., Rupakheti, M., Münkel, C., Lauer, A., Bozem, H., Hoor, P., Butler, T. and Lawrence, M.G. (2017). Investigation of the mixing layer height derived from ceilometer measurements in the Kathmandu Valley and implications for local air quality. *Atmos. Chem. Phys.* 17: 8157–8176.

Ojha, N., Pozzer, A., Rauthe-Schöch, A., Baker, A.K., Yoon, J., Brenninkmeijer, C.A.M. and Lelieveld, J. (2016). Ozone and carbon monoxide over India during the summer monsoon: Regional emissions and transport. *Atmos. Chem. Phys.* 16: 3013–3032.

Panday, A.K. and Prinn, R. G. (2009). Diurnal cycle of air pollution in the Kathmandu Valley, Nepal: Observations. *J. Geophys. Res.* 114: D09305.

Panday, A.K., Prinn, R.G. and Schär, C. (2009). Diurnal cycle of air pollution in the Kathmandu Valley, Nepal: 2. Modeling results. *J. Geophys. Res.* 114: D21308.

Pant, P., Hegde, P., Dumka, U.C., Sagar, R., Satheesh, S.K., Moorthy, K.K., Saha, A. and Srivastava, M.K. (2006). Aerosol characteristics at a high-altitude location in central Himalayas: Optical properties and radiative forcing. *J. Geophys. Res.* 111: D17206.

Putero, D., Landi, T.C., Cristofanelli, P., Marinoni, A., Laj, P., Duchi, R., Calzolari, F., Verza, G. and Bonasoni, P. (2014). Influence of open vegetation fires on black carbon and ozone variability in the southern Himalayas (NCO-P, 5079 m asl). *Environ. Pollut.* 184: 597–604.

Putero, D., Cristofanelli, P., Marinoni, A., Adhikary, B., Duchi, R., Shrestha, S.D., Verza, G.P., Landi, T.C., Calzolari, F., Busetto, M., Agrillo, G., Biancofiore, F., Di Carlo, P., Panday, A.K., Rupakheti, M. and Bonasoni, P. (2015). Seasonal variation of ozone and black carbon observed at Paknajol, an urban site in the Kathmandu Valley, Nepal. *Atmos. Chem. Phys.* 15: 13957–13971.

Raatikainen, T., Hyvärinen, A.P., Hatakka, J., Panwar, T., Hooda, R., Sharma, V. and Lihavainen, H. (2014). The effect of boundary layer dynamics on aerosol properties at the Indo-Gangetic plains and at the foothills of the Himalayas. *Atmos. Environ.* 89: 548–555.

Ram, K., Sarin, M.M. and Hegde, P. (2010). Long-term record of aerosol optical properties and chemical composition from a high-altitude site (Manora Peak) in Central Himalaya. *Atmos. Chem. Phys.* 10: 11791–11803.

Ramanathan, V., Li, F., Ramana, M., Praveen, P., Kim, D., Corrigan, C., Nguyen, H., Stone, E.A., Schauer, J.J.,

Carmichael, G., Adhikary, B. and Yoon, S.C. (2007). Atmospheric brown clouds: Hemispherical and regional variations in long-range transport, absorption, and radiative forcing. *J. Geophys. Res.* 112: D22.

Rupakheti, D., Adhikary, B., Praveen, P.S., Rupakheti, M., Kang, S., Mahata, K.S., Naja, M., Zhang, Q., Panday, A.K. and Lawrence, M.G. (2017). Pre-monsoon air quality over Lumbini, a world heritage site along the Himalayan foothills. *Atmos. Chem. Phys.* 17: 11041–11063.

Sandholz, S. (2016). Potential for ecosystem-based disaster risk reduction and climate change adaptation in the urban landscape of Kathmandu Valley, Nepal. In *Ecosystem-based disaster risk reduction and adaptation in practice*. Springer, pp. 335–360.

Seidel, D.J., Zhang, Y., Beljaars, A., Golaz, J.C., Jacobson, A.R. and Medeiros, B. (2012). Climatology of the planetary boundary layer over the continental United States and Europe. *J. Geophys. Res.* 117: D17106.

Seinfeld, J. (2008). Atmospheric science: Black carbon and brown clouds. *Nat. Geosci.* 1: 15–16.

Shindell, D., Kuylenstierna, J.C.I., Vignati, E., van Dingenen, R., Amann, M., Klimont, Z., Anenberg, S.C., Muller, N., Janssens-Maenhout, G., Raes, F., Schwartz, J., Faluvegi, G., Pozzoli, L., Kupiainen, K., Höglund-Isaksson, L., Emberson, L., Streets, D., Ramanathan, V., Hicks, K., Oanh, N.T.K., Milly, G., Williams, M., Demkine, V. and Fowler, D. (2012). Simultaneously mitigating near-term climate change and improving human health and food security. *Science* 335: 183–189.

Sinha, B., Singh Sangwan, K., Maurya, Y., Kumar, V., Sarkar, C., Chandra, B.P. and Sinha, V. (2015). Assessment of crop yield losses in Punjab and Haryana using 2 years of continuous in situ ozone measurements (2015). *Atmos. Chem. Phys.* 15: 9555–9576.

Sprenger, M. and Wernli, H. (2015). The LAGRANTO Lagrangian analysis tool – version 2.0. *Geosci. Model Dev.* 8: 2569–2586.

Stockwell, C.E., Christian, T.J., Goetz, J.D., Jayarathne, T., Bhave, P.V., Praveen, P.S., Adhikari, S., Maharjan, R., DeCarlo, P.F., Stone, E.A., Saikawa, E., Blake, D.R., Simpson, I.J., Yokelson, R.J. and Panday, A.K. (2016). Nepal Ambient Monitoring and Source Testing Experiment (NAMaSTE): Emissions of trace gases and light-absorbing carbon from wood and dung cooking fires, garbage and crop residue burning, brick kilns, and other sources. *Atmos. Chem. Phys.* 16: 11043–11081.

ul-Haq, Z., Tariq, S. and Ali, M. (2015). Tropospheric NO_2 trends over South Asia during the last decade (2004–2014) using OMI data. *Adv. Meteorol.* 2015: 1–18.

UNEP and WMO (2011). Integrated assessment of black carbon and tropospheric ozone, Nairobi, Kenya.

van Zelm, R., Preiss, P., van Goethem, T., Van Dingenen, R. and Huijbregts, M. (2016). Regionalized life cycle impact assessment of air pollution on the global scale: Damage to human health and vegetation. *Atmos. Environ.* 134: 129–137.

von Engeln, A. and Teixeira, J. (2013). A planetary boundary layer height climatology derived from ECMWF reanalysis data. *J. Clim.* 26: 6575–6590.

Wernli, B.H. and Davies, H.C. (1997). A Lagrangian-based analysis of extratropical cyclones. I: The method and some applications. *Q. J. R. Meteorol. Soc.* 123: 467–489.

Xu, Y., Ramanathan, V. and Washington, W.M. (2016). Observed high-altitude warming and snow cover retreat over Tibet and the Himalayas enhanced by black carbon aerosols. *Atmos. Chem. Phys.* 16: 1303–1315.